Constraining Radio Mode Feedback in Galaxy Clusters with the Cluster Radio AGN Properties to $z\sim1$

Nikhel Gupta[1,2], Maurilio Pannella[2], Joe Mohr[2] + DES + SPT

1) School of Physics, University of Melbourne, Parkville, VIC 3010, Australia
2) Faculty of Physics, Ludwig-Maximilians-Universität, Scheinerstr. 1, 81679 Munich, Germany
(+ 39 institutions)

Abstract

- We study the properties of the Sydney University Molonglo Sky Survey (SUMSS) 843 MHz radio AGN population in galaxy clusters from two large catalogs created using the Dark Energy Survey (DES). The first contains ∼11,800 optically selected redMaPPer clusters (RM-Y3; $M_{200c} > 10^{14}M_{\odot}$, $z < 0.8$) and the second contains ∼1,000 X-ray selected clusters from the ROSAT All Sky Survey (MARD-Y3; $M_{200c} > 2\times10^{14}M_{\odot}$, $z < 1$).
- We show that cluster radio loud active galactic nuclei (AGN) are highly concentrated around cluster centers to $z\sim1$.
- We measure the halo occupation number for cluster radio AGN above a threshold luminosity.
- Using optical counterparts for these sources, we demonstrate weak redshift evolution in the host broad band colors and the radio luminosity at fixed host galaxy stellar mass. We use the redshift evolution in radio luminosity to break the degeneracy between density and luminosity evolution scenarios in the redshift trend of the radio AGN luminosity function (LF).
- The LF exhibits a redshift trend of the form $(1+z)^{\gamma}$ in density and luminosity of $\gamma = 3.0\pm0.4$ and $\gamma = 0.21 \pm 0.15$, respectively, in the RM-Y3 sample, and $\gamma = 2.6 \pm 0.7$ and $\gamma = 0.31\pm0.15$, respectively, in the MARD-Y3 sample.
- We use the cluster radio galaxy LF to estimate the average radio-mode feedback energy as a function of cluster mass and redshift and compare it to the core ($< 0.1R_{500c}$) X-ray radiative losses for clusters at $z < 1$.

Data

Galaxy Clusters

RM-Y3:
•Built using DES Y3 GOLD-release multiwavelength catalog, which covers ∼ 5000 deg^2 of the southern sky.
•Contains ∼11,800 optically selected redMaPPer clusters (RM-Y3; $M_{200c} > 10^{14}M_{\odot}$, $z < 0.8$) with median mass and redshift of $1.52 \times 10^{14}\ M_{\odot}$ and 0.47, respectively.
•Masses estimated using McClintock et al. (2019) relation.

MARD-Y3:
•Contains ~1,000 X-ray selected ROSAT All Sky Survey (RASS) cluster catalog (Klein et al. 2019).
•Masses estimated using scaling relations from Bulbul et al. (2019) with median mass and redshift of $5.06 \times 10^{14}\ M_{\odot}$ and 0.28, respectively.

Radio Galaxy Catalog

•Sydney University Molonglo Sky Survey (**SUMSS**; Bock et al. 1999; Mauch et al. 2003; Murphy et al. 2007) imaged the southern radio sky at 843 MHz.
•Contains 210,412 AGN to a limiting peak brightness of 6 mJy beam^{-1} at $\delta\leq-50^{\circ}$ and 10 mJy beam^{-1} at $\delta>-50^{\circ}$.

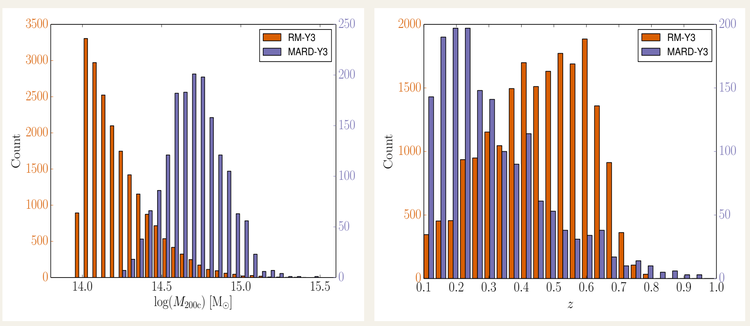

Figure 1 Distribution of RM-Y3 and MARD-Y3 galaxy clusters as a function of mass (left panel) and redshift (right panel).

AGN Optical Counterpart Identification

- We derive stellar masses (M_*) for all the objects in sample.
- Examine the surface density of DES sources as a function of their distance from the SUMSS AGN for different bins of stellar mass.
- Chose top two bins (log $M_* > 11.3$ and $11.3 >$ log $M_* > 10.9$) and a maximum offset of 10" and 6".
- Assign cluster membership to the radio AGN by comparing the DES photometric redshift of each source to the redshift of the cluster.
- We find 2,264 candidate cluster radio AGN that lie within the radius θ_{200} of RM-Y3 clusters.

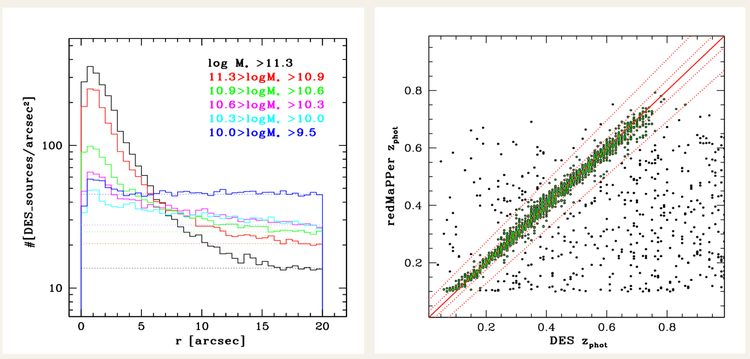

Figure 2 Surface number density of DES galaxies as a function of the offset from SUMSS AGN for different stellar mass ranges (left panel). Comparison between RM-Y3 cluster redshifts and the photo-z of SUMSS counterparts (right panel).

AGN Stellar-Mass and Luminosity Relation

Constrain stellar-mass to radio AGN luminosity relation for high power sources (log [P/(W Hz^{-1})] > 25.3) in galaxy clusters.

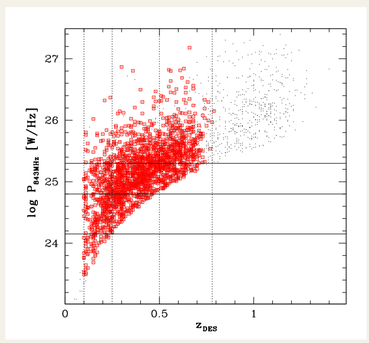

Fit for the power law relation:

$$P_{843\mathrm{MHz}} = 10^{A_{\mathrm{PM}}}\left(\frac{M_*}{M_{*,\mathrm{piv}}}\right)^{B_{\mathrm{PM}}}\left(\frac{1+z}{1+z_{\mathrm{piv}}}\right)^{\gamma_{\mathrm{PM}}},$$

$M_{*,piv} = 3.7 \times 10^{11}\ M_{\odot}$
$z_{piv} = 0.51$

$A_{PM} = 25.51 \pm 0.006$
$B_{PM} = 0.01 \pm 0.02$
$\gamma_{PM} = 0.30 \pm 0.15$

Figure 3 Luminosity distribution of SUMSS sources observed at 843 MHz as a function of redshift. The black points show radio sources inside θ_{200} of RM clusters, the red squares show instead the radio sources identified as cluster members.

Cluster AGN Surface Density Profiles

- We study the radial distribution of radio AGN in the cluster θ_{200c} region by stacking the AGN overlapping the cluster samples.
- We fit NFW model finding centrally concentrated profile with $c = 143\pm10$ and 144 ± 30 for the RM-Y3 and MARD-Y3 samples.
- We find lower concentrations of radio AGN in clusters at higher redshifts with $c = 250\pm40$, 141 ± 21 and 107 ± 18 for low to high redshift bin.

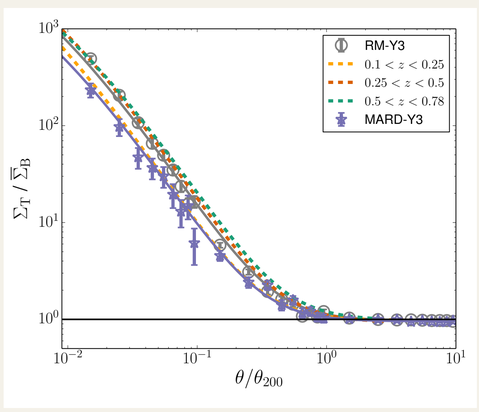

Figure 4 The projected radial distribution of radio AGN observed at 843 MHz around the centers of the optically selected RM-Y3 (gray) and X-ray selected MARD-Y3 (blue) galaxy clusters.

Cluster AGN Luminosity Functions

- We construct cluster AGN luminosity functions (LFs) in the direction of the optically selected RM-Y3 and the X-ray selected MARD-Y3 galaxy clusters.
- Perform statistical background corrections to estimate cluster AGN number counts.
- Fit the LF in redshift bins using Condon et al. (2002) fitting functions, given as:

$$\log\left(\frac{\mathrm{d}n}{\mathrm{d}\log P}\right) = y - \left[b^2 + \left(\frac{\log P - x}{w}\right)^2\right]^{1/2} - 1.5\log P,$$

- The density evolution corresponds to a vertical shift in the LFs and can be quantified as

$$\frac{\mathrm{d}n(z)}{\mathrm{d}\log P} = \frac{\mathrm{d}n(z=z_{\mathrm{C}})}{\mathrm{d}\log P} \times \left(\frac{1+z}{1+z_{\mathrm{C}}}\right)^{\gamma_{\mathrm{D}}},$$

- The luminosity evolution corresponds to a horizontal shift in the LFs because of the evolving luminosities of the sources

$$P(z) = P(z=z_{\mathrm{C}}) \times \left(\frac{1+z}{1+z_{\mathrm{C}}}\right)^{\gamma_{\mathrm{P}}},$$

- We use $\gamma_{PM} = 0.30 \pm 0.15$ from cluster AGN stellar-mass to luminosity relation as a prior to jointly fit density and luminosity evolution in the LFs.

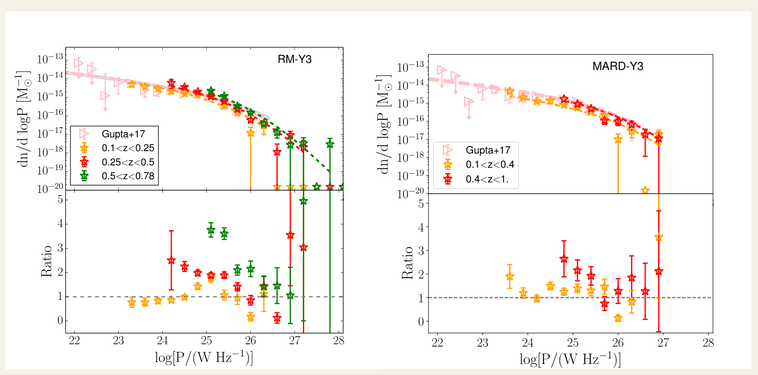

Figure 5 SUMSS based 843 MHz cluster radio AGN LFs observed from RM-Y3 (left) and MARD-Y3 (right) catalogs. Upper panels show the LFs obtained using the statistical background subtraction. Pink points and line represent the best fit model and model uncertainties from Gupta et al. (2017). Lower panels show the ratio between the measurements and the best fit model for the lowest redshift bin in this work.

y	x	γ_{D}	γ_{P}
RM-Y3			
25.82 ± 0.04	26.56 ± 0.06	3.16 ± 0.43	–
25.82 ± 0.04	26.56 ± 0.06	–	3.16 ± 0.42
25.75 ± 0.04	26.40 ± 0.06	3.00 ± 0.42	0.21 ± 0.15
MARD-Y3			
25.83 ± 0.12	26.86 ± 0.14	2.60 ± 0.71	–
25.82 ± 0.12	26.84 ± 0.14	–	2.62 ± 0.70
25.74 ± 0.11	26.70 ± 0.15	2.05 ± 0.66	0.31 ± 0.15

Table 1 The best fit LF parameters for different samples of cluster radio AGN. γ^D and γ^P are defined as the density and luminosity redshift evolution parameters, respectively. The joint constraints on γ^D and γ^P are obtained when a Gaussian prior on γ^P is adopted from the best fit redshift evolution of the stellar mass - luminosity relation.

Halo Occupation Number

- Halo Occupation Number (HON) is the average number of background subtracted radio AGN per cluster.
- We estimate the HON in a stack of RM-Y3 and MARD-Y3 clusters in various mass bins to study the mass trends for observed cluster radio sources.

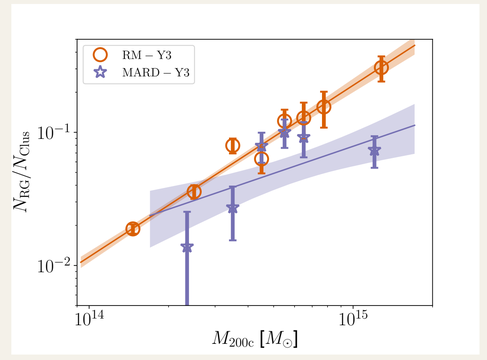

Figure 6 The mean number of radio sources with log [P/(W Hz^{-1})] > 25.5 per galaxy cluster as a function of cluster mass at $z = 0.47$ using optically selected RM-Y3 (red) and X-ray selected MARD-Y3 (blue) clusters. The solid line is the best fit power law model and the shaded region shows the 1-σ model uncertainty.

- The best fit power law is of the form:

$$N_{\mathrm{RG}} = A_{\mathrm{H}}\left(\frac{M_{200\mathrm{c}}}{1.5\times10^{14}}\right)^{B_{\mathrm{H}}}\left(\frac{1+z}{1+z_{\mathrm{C}}}\right)^{\gamma_{\mathrm{D}}},$$

N_{RG} describes the average number of radio AGN in a cluster with log[P/(W Hz^{-1})] > 25.5.

$B_H = 1.2\pm0.1$ (RM-Y3)
$B_H = 0.68\pm0.34$ (MARD-Y3)

Radio Mode Feedback

- We calculate the mean total cluster radio AGN power P_{Radio} using our measured LF from the analysis of the RM-Y3 sample.
- We use the Cavagnolo et al. (2010) relation to estimate the cavity power P_{cav} that represents an estimate of the minimum mechanical feedback into the intra cluster medium (ICM).

$$\mathrm{P_{cav}} = 5\times10^{43}\left(\frac{L1400}{10^{40}\ \mathrm{erg\ s^{-1}}}\right)^{0.7}\ \mathrm{erg\ s^{-1}}.$$

- We use the measurements of the core luminosities from Bulbul et al. (2019) together with mass and redshift measurements for the subset of the galaxy cluster sample where the core region of interest is larger than the XMM-Newton point spread function.
- The best fit core ($\leq 0.1R_{500}$) X-ray luminosity to mass relation that we find is

$$\mathrm{P_{Xray}} = 16.88^{+1.53}_{-1.40}\times10^{44}\mathrm{erg\ s^{-1}}\left(\frac{M_{500}}{M_{\mathrm{piv}}}\right)^{2.4\pm0.2}\left(\frac{E(z)}{E(z_{\mathrm{piv}})}\right)^{7/3}\left(\frac{(1+z)}{(1+z_{\mathrm{piv}})}\right)^{-0.7\pm0.4},$$

- The ratio between the radio cavity power and the core X-ray luminosity is correlated with the redshift of the clusters and is anti-correlated with its mass.

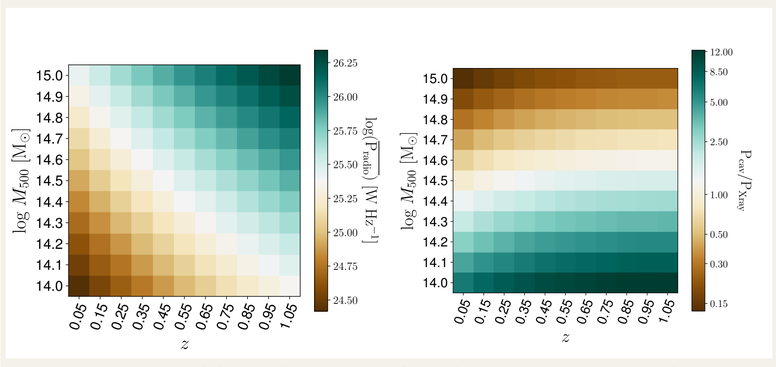

Figure 7 Mean radio power at 843 MHz (left) of cluster radio AGN as a function of cluster mass and redshift calculated using the radio LF. On the right, we plot the ratio of the estimated mechanical feedback energy P_{cav} from the radio AGN to the central X-ray luminosities ($r < 0.1R_{500}$) from the ICM as a function of cluster mass and redshift. The ratio of the radio feedback to X- ray radiative losses for a $10^{14}M_{\odot}$ galaxy cluster is ∼ 2 times larger at $z \sim 1.05$ as compared to the ratio at $z \sim 0.05$.

References

- Bock D. C.-J., Large M. I., Sadler E. M., 1999, AJ, 117, 1578
- Bulbul E., et al., 2019, ApJ, 871, 50
- Cavagnolo K. W., McNamara B. R., Nulsen P. E. J., Carilli C. L., Jones C., Bîrzan L., 2010, ApJ, 720, 1066
- Condon J. J., Cotton W. D., Broderick J. J., 2002, AJ, 124, 675
- Gupta N., et al., 2017, MNRAS, 467, 3737
- Klein M., et al., 2019, MNRAS, p. 1397
- Mauch T., Murphy T., Buttery H. J., Curran J., Hunstead R. W., Piestrzynski B., Robertson J. G., Sadler E. M., 2003, MNRAS, 342, 1117
- McClintock T., et al., 2019, MNRAS, 482, 1352
- Murphy T., Mauch T., Green A., Hunstead R. W., Piestrzynska B., Kels A. P., Sztajer P., 2007, MNRAS, 382, 382

Contact Information

Corresponding author: Dr Nikhel Gupta
Address: School of Physics, University of Melbourne, Parkville, VIC 3010, Australia
E-mail: nikhel.gupta@unimelb.edu.au